Coarsening kinetics in demixed lead borate melts

A. Dittmar, H. Bornhöft, and J. Deubener

Citation: The Journal of Chemical Physics **138**, 224502 (2013); doi: 10.1063/1.4808162
View online: http://dx.doi.org/10.1063/1.4808162
View Table of Contents: http://scitation.aip.org/content/aip/journal/jcp/138/22?ver=pdfcov
Published by the AIP Publishing

Coarsening kinetics in demixed lead borate melts

A. Dittmar, H. Bornhöft, and J. Deubener[a)]
Institute of Non-Metallic Materials, Clausthal University of Technology, 38678 Clausthal-Zellerfeld, Germany

(Received 30 March 2013; accepted 16 May 2013; published online 10 June 2013)

Lead borate melts have been demixed at temperatures in range from 723 to 773 K for times up to 20 h. It is found that increasing time and temperature lead to characteristic changes in the size distribution of boron trioxide drops in the lead-rich glassy matrix (<80.7 mol. % B_2O_3). The increase of the mean drop size with annealing time followed the cube root time dependence of diffusion controlled coarsening. The diffusivity of the coarsening process was determined using liquid-liquid interfacial energy associated with drop deformation in glass specimens subjected to uniaxial compression. Diffusion coefficients of coarsening were found to match with those of ^{207}Pb and ^{18}O tracer ions in the lead borate system but differ up to four orders of magnitude from the Eyring diffusivity and by a factor of ≈7 from the activation energy of viscous flow. The results indicate that coarsening in demixed lead borate melts is most likely controlled by the short range dynamics of the interaction between lead cations and BO_4 units, which are decoupled from the time scales of cooperative rearrangements of the glassy network at $T < 1.1\ T_g$. © *2013 AIP Publishing LLC*. [http://dx.doi.org/10.1063/1.4808162]

I. INTRODUCTION

Nanosized structures in glasses of embedded amorphous and crystalline phases result mostly from first order transitions of the supersaturated and supercooled liquid state. In both cases final competitive growth of particles and drops, i.e., Ostwald ripening, will create a coarser texture by increasing the size and decreasing the number density of participates in a self similar process. Therefore, limiting Ostwald ripening is fundamental in material engineering to develop structures with precipitates in the range of nanometers.

A. Coarsening rate calculations

The microstructure of phase separated glasses can be tailored in general by controlling the kinetics of the Ostwald ripening process. In particular, diffusion controlled ripening was assumed by fitting mean drop radii $\bar{r}$ of small angle x-rays and neutron scattering (SAXS, SANS),[1,2] transmission and scanning electron microscopy (TEM, SEM),[3–5] and atomic force microscopy (AFM)[6] studies to the cubic root time dependence $t^{1/3}$. Calculations of the coarsening rate K were impeded particularly by the lack of the liquid-liquid interfacial energy σ_{ll} for most systems. In a first approach viscosity derived diffusivity data were used to determine the interfacial energy by assuming coupled characteristic time scales of coarsening and viscosity.[5] Further, the ratio of growth and coarsening rate of the demixing process was utilized to determine the liquid-liquid interfacial energy.[7] This method anticipates the same rate controlling species in both stages of the demixing process. Furthermore, different experimental approaches were reported to determine σ_{ll} independent of ripening theory analyzing size[8] and shape of segregated drops,[2,9] which allows in principle the calculation of the coarsening rate if diffusivity of the movable species is known. However, the coarsening kinetics in these systems has not been reported. Thus, we have combined in this study for the first time measurements of both coarsening rate and liquid-liquid interfacial energy to predict the rate controlling species of the coarsening process. Therefore, demixed glasses of the binary lead borate system were used.

B. Immiscibility in the PbO-B_2O_3 system

Stable liquid immiscibility is evident in the PbO-B_2O_3 system for temperatures below 1058 K in a narrow compositional range from approx. 100 to 80 mol. % B_2O_3.[10,11] For temperatures below 1015 K the dome of the demixing curve is prolonged by two descending branches corresponding to the metastabile equilibrium of sub-liquidus temperatures.[1,12,13] Figure 1 shows the immiscibility as well as the transition temperatures of the corresponding end member glasses in the lead borate system. Binodal temperatures were based on a modified regular solution model[14] using equilibrium compositions of pure boron trioxide and lead tetraborate.[15] Experimental investigation showed drops-in-matrix microstructures and no evidence of an interconnected morphology although the phase-separation process should proceed via spinodal decomposition in the central part of the immiscibility dome.[16,17] Further, gravity induced segregation of the microstructure (minimized only under μ-gravity condition) was observed.[18–20] Physical properties of the phase-separated glasses revealed a sharp transition from a morphology consisting of lead-rich drops in a nearly pure B_2O_3 matrix to lead-depleted drops in a matrix of approx. 20 mol. % PbO. Deformability of the two liquids under external forces was reported in rheological and dilatometric studies for temperatures above 723 K.[17,21]

According to the partially stable nature of the immiscibility in the PbO-B_2O_3 system the kinetics of drop growth is fast for cooling of the first 43 K, i.e., the difference between critical and liquidus temperature. The phase

a)Electronic mail: joachim.deubener@tu-clausthal.de.

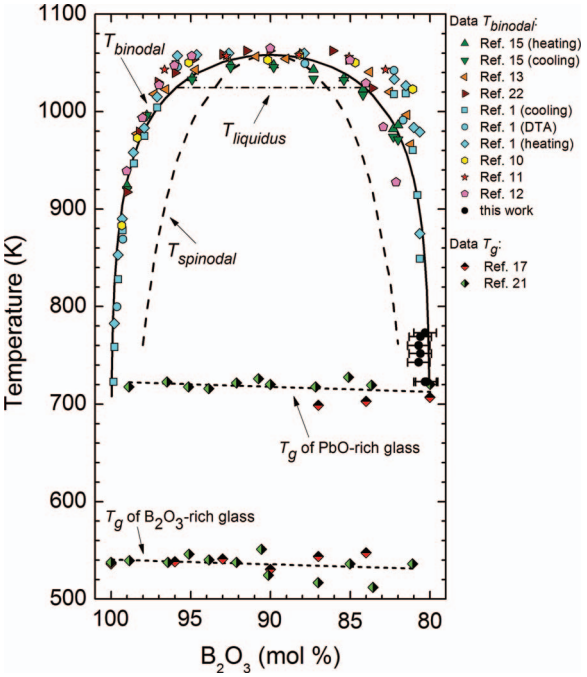

FIG. 1. Miscibility gap in the PbO-B_2O_3 system. Data according to different authors as indicated. Binodal temperatures (solid line) were fitted using the modified regular solution model of Simmons,[15] the critical temperature (1058 K[11]), and the equilibrium compositions B_2O_3 and $PbO \cdot 4B_2O_3$. Reduced mixing entropy ($\Delta S/R = 7.2 \pm 0.3$) was adjusted to obtain the best line through the data. The liquidus temperature $T_{liq} = 1015$ K (dashed-dotted line) was redrawn from Geller and Bunting.[10] The dashed lines illustrate the best straight lines through the data of the transition temperature T_g of the B_2O_3-rich and PbO-rich glasses.

separation rate was estimated from *in situ* measurements to be at least 900 times larger than that of the metastable phase separation below the liquidus.[22] Consequently, drop-in-matrix microstructures are frozen-in from regular cooling rates ($<10^2$ K min^{-1}). Besides gravity induced segregation annealing above the two glass transition temperatures led to coarsening of the microstructure.

C. Structure of lead borate glasses

The structure of lead borate glasses has been studied *inter alia* by ^{11}B and ^{207}Pb magic angle spinning NMR,[23,24] and IR spectroscopy.[25] Both methods showed that the addition of PbO (up to 40 mol. %) into the B_2O_3 network led to an increase in the fraction of 4-coordinated boron (N_4). The conversion of BO_3 units to BO_4 units in lead borate glasses is associated with two distinct sites for the Pb^{2+} ion environment. In a lead triborate (75 mol. % B_2O_3) glass the first site exhibits a 7-8 fold coordination to oxygen, while the second has coordination number = 4-6.[24] Therefore, the Pb^{2+} ion acts mainly as a charge compensator filled in the interspaces between the different BO_4 containing borate groups.

To predict the rate controlling species the paper aims in determining the coarsening rate K of nano-sized B_2O_3-rich drops in a PbO-rich matrix from the temporal evolution of their size distribution, but also from the rate law utilizing liquid-liquid interfacial energy data, which were determined independently from the coarsening theory by emulsion rheology for this glass composition. In particular, we want to answer the question: Is the coarsening kinetics in demixed glass melts coupled with the network mobility? To shed light on the coarsening mechanism we derived diffusivity data from both ion diffusion and viscosity.

II. METHOD

A. Coarsening theory

The overall process of coarsening is driven by the reduction of the total free energy of the system and proceeds due to curvature supercooling/supersaturating via heat and mass transport. In the absence of convective effects the diffusion of the precipitated phase is assumed to control the coarsening kinetics as analyzed by Lifshitz and Slyozov[26] and Wagner[27] (herein named as LSW-theory). Ratke and Thieringer[28] showed that in the case of a pure diffusion-controlled ripening without drop moving the rate constant K of the growth of the mean particle can be expressed by the difference of the equilibrium compositions as

$$K = K_{LSW} = \frac{\bar{r}^3(t) - \bar{r}_0^3}{t} = \frac{8\sigma_{ll} D V_m}{9RT} \frac{c^\alpha}{(c^\beta - c^\alpha)}, \qquad (1)$$

where $\bar{r}_0$ and $\bar{r}(t)$, respectively, are the initial and actual mean drop radii of the coarsening stage at time $t = 0$ and t, ; σ_{ll} is the liquid-liquid interfacial energy; D is the diffusion coefficient of the moving species through the interface; V_m is the molar volume of the drop phase; R is the gas constant; T is the absolute temperature; and c^α, c^β are the concentrations of the solute at the interface outside the drop and in the drop, respectively.

The LSW theory is only valid in the limit of a zero-volume fraction of coarsening phase. Theoretical work has been done to address this critical shortcoming. Modern theories determine the statistically averaged growth rate for a drop of given size but differ in the methodology of this calculation. Among these are the MLSW,[29] BW,[30] LSEM,[31] TM,[32] MR,[33] TK,[34] and VG[35,36] theory, which are compared comprehensively by, e.g., Voorhees[37] and Baldan.[38] All these theories predict that a finite volume fraction of the precipitate does not alter the temporal exponent of the average drop radius from the LSW prediction of 1/3. In contrast, a strong dependency of the coarsening rate K on volume fraction is computed

$$K(\phi) = K_{LSW} \Phi(\phi), \qquad (2)$$

where $\Phi(\phi)$ is the system-independent correction function of the precipitated volume fraction ϕ.

The time-invariant LSW drop size distribution is highly asymmetric with a sharp cut-off at 1.5 $r/\bar{r}$. Models for $\phi > 0$ predict volume fraction-dependent drop size distributions becoming broader and more symmetric with increasing ϕ. However, the form of the steady-state drop size distribution differs from theory to theory.

B. Liquid-liquid interfacial energy

Classical theories of emulsion rheology yield information on the deformation of a liquid drop dispersed into

another liquid matrix phase. By connecting the deformation and the capillary number of the dispersed phase interfacial energy can be estimated. Capillary number Ca specifies the balance of the external stresses, which act to deform the surface, and the interfacial energy, which tends to keep the drop spherical:

$$Ca = \frac{\eta_m r \dot{\varepsilon}}{\sigma_{ll}}, \tag{3}$$

where η_m is the viscosity of the matrix phase, $\dot{\varepsilon}$ is the external strain rate, σ_{ll} is the interfacial energy between drop and matrix phase, and r is the capillary radius of the initially spherical particles, $r = L^{1/3}B^{2/3}$. Assuming a rotational symmetric elipsoidic shape, the ovality δ is then given by

$$\delta = \frac{L - B}{L + B}, \tag{4}$$

where L and B, respectively, are the longest/shortest semiaxes of the elipsoidic drop after deformation, and utilizing the Cox relation (modified Navier-Stokes equation)

$$\delta = 5\,(19\kappa + 16)\left[4\,(1+\kappa)\sqrt{(19\kappa)^2 + \left(\frac{20}{Ca}\right)^2}\right]^{-1}, \tag{5}$$

with $\kappa = \eta_d / \eta_m$ (η_d = viscosity of the drop) one obtains for the interfacial energy[9]

$$\sigma_{ll} = \frac{\eta_m \dot{\varepsilon} \sqrt[3]{LB^2}}{20}\sqrt{\left(\frac{5\,(19\kappa + 16)}{4\delta\,(1+\kappa)}\right)^2 - (19\kappa)^2}. \tag{6}$$

C. Diffusivity

If the diffusing species interacts strongly with the melt structure or is a network-forming ion the relation between viscosity and diffusion has the functional form of the classic Eyring equation:[39]

$$D_\eta = \frac{kT}{\lambda\eta}, \tag{7}$$

where k is the Boltzmann constant and λ is the jump distance. In the Eyring model, diffusion of a particle (atom, ion) is based on a hop or a jump, which results when the nearest neighbours of the diffusive particle are pushed aside. Eyring treads the short-range order in liquids as a quasi-lattice structure in small regions and allows the particle to jump out of the potential wall into its adjacent hole. The size of the activated complex λ, containing $Cn + 1$ particle, is related to[39]

$$\lambda = Cn\left(\frac{V_M}{mN_A}\right)^{1/3}, \tag{8}$$

where V_M and Cn are the molar volume and the coordination number of the moving particle in the cluster, respectively, N_A is Avogadro number, and m is the number of atoms per formula unit.

If the diffusing species can make diffusive jumps without requiring cooperative rearrangement of the melt structure, the diffusivity is entirely decoupled from melt viscosity and follows an Arrhenian temperature dependence, i.e.,

$$D_i = D_0 \exp\left(B/kT\right), \tag{9}$$

where the constants B and D_0 are, for each species, different and can be related to their charge and radius as well as the composition of the melt. In order to obtain the diffusivity from coarsening rates one may rewrite Eq. (1) using Eq. (2):

$$D_K = \frac{K}{\Phi(\phi)}\frac{9RT}{8\sigma_{ll}V_m}\frac{(c^\beta - c^\alpha)}{c^\alpha}. \tag{10}$$

III. EXPERIMENTAL

A. Glass preparation and composition

Three glasses of the nominal molar composition 16PbO, $84B_2O_3$ (PB1, PB2), and 18PbO $82B_2O_3$ (PB3) were prepared by mixing analytical grade powders of boric acid (Riedel de Haën, >99%) and lead^{II,IV} oxide (Riedel de Haën, >96%). Batches of 75 g were molten in covered platinum crucibles in an electrical heated furnace (Nabertherm LHT04/17, Lilienthal, Germany) at 1223 K for 1 h (PB1, PB3) and at 1393 K for 3 h (PB2), while stirred periodically. Thereafter the melts were clear and homogeneous and decantation in the crucible due to lead reduction was not observed. The fused glasses were cast in cylindrical graphite moulds, annealed in a muffle at 723 K for 2 h, and finally slowly cooled to room temperature (≈3–5 K min^{-1}) by shutting of the heating. Fractured surfaces revealed a drop-in-matrix microstructure of PB1 and PB2 glass, whereas PB3 glass was drop-free after cooling.

The actual composition of the glasses was determined from their density ρ using a helium pycnometer (Porotec Pycnomatic ATC, Hofheim, Germany) at room temperature and utilizing the compositional dependence of ρ in the lead borate system.[16] The B_2O_3 content was 82.2 (PB1), 81.8 (PB2), and 79.8 (PB3) mol. % (error = 0.5 mol. %), which indicated volatilization of ≈2 mol. % of boron trioxide due to the applied melting condition (Table I).

The water content of the demixed lead borate glasses PB1 and PB2 was determined from the thickness corrected absorbance (E/d) at the OH vibration band maximum close to 3550 cm^{-1} and using an effective absorption coefficient of 0.0218 (ppmw OH)$^{-1}$ cm^{-1} of a lead borate glass with 20 mol. % PbO.[40] Absorbance of polished glass specimens (thickness d = 0.210 cm (PB1) and 0.167 cm (PB2)) was measured in the near infrared region at wave numbers from 2000 to 5000 cm^{-1} using an FT-IR spectrometer (Vertex 70, Bruker AXS, Billerica, USA) in air at room temperature. The absorption intensity at the band maximum close to 3550 cm^{-1} resulted in a relative small retention of water, i.e., 780 (PB1) and 700 (PB2) ppmw OH (Fig. 2). Thus, we assume that the effects of water on immiscibility and coarsening were relatively small and of comparable size for all glasses of this study.

B. Uniaxial compression experiments

The demixed glasses PB1 and PB2 were uniaxially compressed in a vertical dilatometer (Bähr VIS404, Hüllhorst,

TABLE I. Density ρ, composition $c^0{}_{B_2O_3}$ of the initial supersaturated glasses PB1, PB2, and the homogeneous glass PB3, drop fraction ϕ, B_2O_3 content of drop $c^\alpha{}_{B_2O_3}$ and matrix $c^\beta{}_{B_2O_3}$ in phase separated glasses PB1 and PB2 after dwelling at temperatures in the range from 723 to 773 K load-free (coarsening regimes) and under load (compression experiments under axial compressive stress σ_{ax}), effective strain rate $\dot{\varepsilon}_{yz}$, drop ovality δ and liquid-liquid interfacial energy σ_{ll}. Number in parenthesis gives uncertainty of the last digit.

Glass	ρ (g cm^{-3})	$c^0{}_{B_2O_3}$ (mol. %) Ref. 16	T (K)	σ_{ax} (MPa)	ϕ (vol. %)	$c^\alpha{}_{B_2O_3}$ (mol. %) Fig. 1	$c^\beta{}_{B_2O_3}$ (mol. %)	δ	$\dot{\varepsilon}_{yz} \times 1000$ (s^{-1})	σ_{ll} (J m^{-2})
PB1	3.117(7)	82.2(5)	723	…	12(1)	99.96	80.3(7)	0.05	…	…
			773	…	12(1)	99.90	80.3(7)	0.04	…	…
			773	0.055	11(1)	99.90	80.4(7)	0.15	0.23(2)	0.016(5)
PB2	3.150(8)	81.8(5)	723	…	10(1)	99.96	80.2(7)	0.07	…	…
			743	0.138	7(1)	99.94	80.7(7)	0.27	0.013(1)	0.019(5)
			752	0.131	8(1)	99.93	80.6(7)	0.28	0.030(3)	0.015(5)
			760	0.129	7(1)	99.92	80.7(7)	0.29	0.11(1)	0.018(5)
			769	0.131	8(1)	99.91	80.6(7)	0.31	0.34(3)	0.017(5)
PB3	3.323(7)	79.8(5)	773	…	…	…	…	…	…	…

Germany) by force control at 4.91, 5.89, and 9.81 N. Therefore, cylinders of height h_0 and diameter d_0 in the range from 8 to 11 mm were prepared by grinding and polishing. The glass forming experiments were carried out at 743, 752, 760, 769, and 773 K. Temperature was controlled to within ±1 K, limited by the accuracy of the *S*-type thermocouple (located 2–3 mm to the upper surface of the cylinder), temperature gradient, and thermal conductivity effects. A heating rate of 10 K min^{-1} was chosen in all experiments to reach the final temperature. After a dwell time for thermal equilibration, the load was applied on the pushing rod and the cylinder started to deform. The actual height h of the cylinders was recorded continuously by a linear variable displacement transducer. Compression was limited to 1/3 of the initial height h_0 by cooling the cylinders under load to room temperature. As mentioned above forming of other glasses under this type of thermomechanical regime (cooling rate ≈5 K min^{-1} at uniaxial stress $\sigma_{ax} > 0$) result in frozen-in strain and permanent birefringent glass specimens.[41–43]

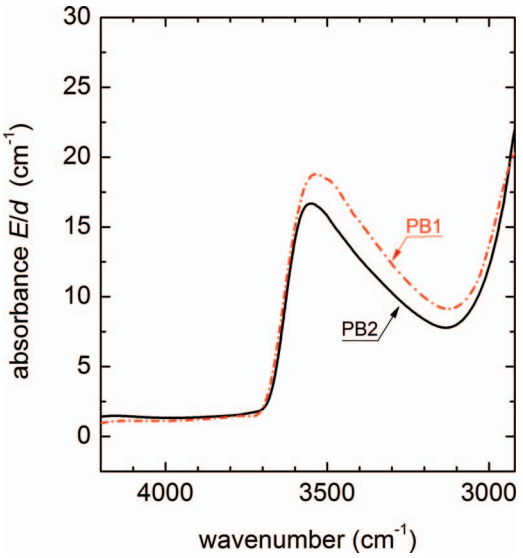

FIG. 2. Absorption in the near infrared region of demixed PB1 and PB2 glasses.

The mean effective strain rate in the equatorial plane of the barrelled cylinder (non-slip condition) was approximated from the normalized compression rate $\dot{\varepsilon}_z = -(\mathrm{d}h/\mathrm{d}t)/h$ in axial direction, the normalized flow rate in the radial direction $\dot{\varepsilon}_y = (\mathrm{d}(d_2/2)/\mathrm{d}t)/(d_2/2)$, and the bulge curvature $R_B = [h^2 + (d_1 - d_2)^2]/4(d_2 - d_1)$, where d_1, d_2 are the minimum and maximum diameters of the barrelled cylinder and h, d are the instantaneous height and diameter of the specimen, respectively.[44] The effective strain rate $\dot{\varepsilon}_{yz} = \sqrt{\dot{\varepsilon_z}^2 + (\xi\dot{\varepsilon}_y)^2}$ at radial position $y = \xi d_2/2$ deviated only slightly (≈10%) from the true strain rate, which was determined by analogue experiments using marked glass cylinders. Marked glass cylinders were prepared from sintered flat glass stacks composed of glass powder between 1 mm thick float glass slides. Those cylinders were compressed under equal rheometric regimes and isokom temperature as the demixed lead borate glasses up to an axial compression $\Delta h/h_0 = 77\%$. From inspection of the shift of the glass powder interfaces in radial direction the true (frozen-in) strain in the equatorial plane was determined (not shown).

C. Viscosity

The viscosity of the liquid-liquid phase-separated glasses PB1 and PB2 was determined during compression of the cylinder using Gent-Equation for non-slip condition:[45]

$$\eta = \frac{F}{3 \cdot V \cdot \dot{h} \cdot \left(\frac{V}{2 \cdot \pi \cdot h^5} + \frac{1}{h^2}\right)}, \tag{11}$$

with F = applied force, V = volume of the cylinder, and $\dot{h} = \mathrm{d}h/\mathrm{d}t$. The viscosity of the homogeneous glass PB3 was determined in the temperature range from 707 K to 773 K by performing micro-indentation experiments. Indentation was performed by attaching a sapphire micro-sphere (radius = 0.75 mm) on the pushing rod head of the vertical dilatometer as used for compression experiments. Accuracy and control of temperature and of the applied heating rate (10 K min^{-1}) were the same as for the cylinder compression experiments. After a dwell time for thermal equilibration, the weight was loaded on the pushing rod and the sphere started

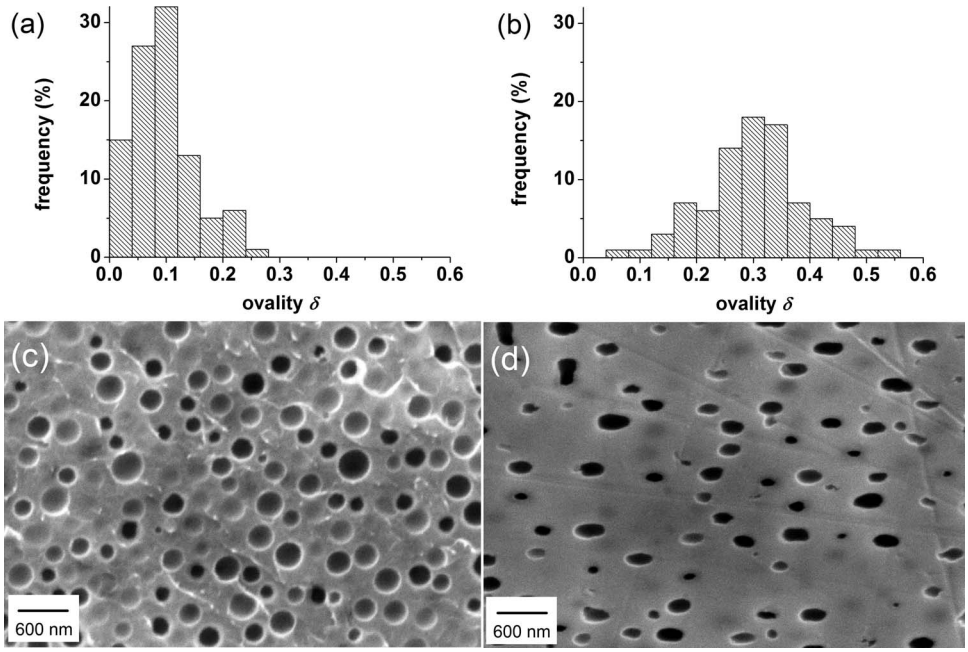

FIG. 3. Secondary electron images of relict structures of demixed drops in lead borate glass matrix. Distribution of drop ovality δ (a) in uncompressed glass PB2 after dwelling at 723 for 2 h (c). Distribution of drop ovality δ (b) in compressed ($\sigma_{ax} = 0.131$ MPa) glass PB2 after dwelling at 769 K and cooling under load (d).

to penetrate the glass surface. A linear variable displacement transducer continuously recorded the indentation depth of the sphere into the glass. The Newtonian shear viscosity η was calculated by[46,47]

$$\eta = \frac{0.1875Ft}{\sqrt{r_S}\sqrt{L^3}}, \tag{12}$$

with F = applied force, t = time, r_S = radius of the sphere, and L = indentation depth. The drop viscosity of the liquid-liquid phase-separated glasses PB1 and PB2 was taken from Dietzel and Brückner[48] assuming a composition of almost pure B_2O_3 of the drops at 743–773 K (Fig. 1). Both viscometers were calibrated using the standard glass (G1) of the PTB (Physikalisch-Technische Bundesanstalt, Germany[49]). The error in viscosity was ± 0.1 log units for micro-indentation and cylinder compression between parallel plates.[50,51]

D. Microstructure

An atomic force microscope AFM (SIS UltraObjective, Herzogenrath, Germany) and a scanning electron microscope SEM (EVO 50, Zeiss, Oberkochen, Germany) were used to determine the size distribution and ovality of drops in the demixed glasses PB1 and PB2. Therefore, glasses were fractured (AFM), polished, and Au-coated (SEM) normal to the equatorial plane of the cylinder. For uncompressed and compressed glasses three-dimensional size distributions of drops were estimated from two-dimensional populations of at least 120 drops per image using ImageJ software (http://rsb.info.nih.gov/ij/) and Schwartz-Saltykov correction factors.[52] Mean radii of the corrected drop size distributions were obtained by fitting LSW and normal distribution functions through the data. In particular, we used AFM scans (each 25 μm^2 with resolution of 512 × 512 pixels) at three different radial positions of the equatorial line (PB1) and SEM images (each 21.4 μm^2 with resolution 1019 × 681 pixel) at ten different radial positions of the equatorial line (PB2) to collect δ data and to calculate equivalent radii from elliptical cross sections of deformed drops in compressed PB1 and PB2 glasses (Fig. 3). For determination of the coarsening rate uncompressed cylinders of glass PB1 were heat-treated at 723 K for 2 and 20 h and at 773 K for 4, 7, 10, and 16 h prior to the microscopic investigation.

The B_2O_3 content of the matrix glass $c^{\alpha}{}_{B_2O_3}$ was approximated from the precipitated volume fraction ϕ and the binodal composition of the drop glass $c^{\beta}{}_{B_2O_3}$ of Fig. 1 using the lever rule and the density of the equilibrium compositions B_2O_3 (1.838 g cm^{-1}[16]) and $PbO \cdot 4B_2O_3$ (3.305 g cm^{-1}[16]). The results were compiled in Table I.

We note that the preparation of surfaces by cracking (AFM) in air and polishing in aqueous solutions (SEM) of PB1 and PB2 glass resulted in a hole-in-matrix topography due to the high thermal expansion and low resistance against water of the nearly pure boron trioxide drop glass. Wheaton and Clare[6] reported on similar relict structures of borate drops as a result of surface preparation of demixed sodium borosilicate glasses.

IV. RESULTS

A. Coarsening rate

Inspecting the mean drop radius cubed as a function of the demixing time reveals in agreement with Eq. (1) a linear dependence, while the distribution of radii is broadened to large sizes (Fig. 4). The almost symmetric form of the drop

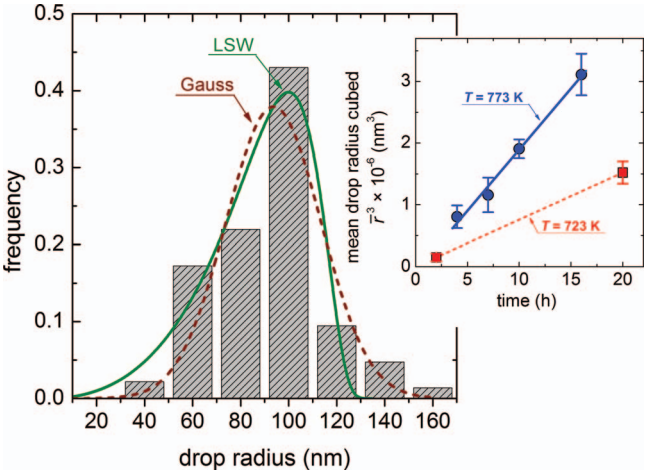

FIG. 4. Size distribution of drops of the demixed glass PB1 after heat treatment at 773 K for 4 h. Mean radius $\bar{r}$ is determined from fitting a Gaussian function through the data. (Inset) Mean radius cubed $\bar{r}^3$ vs. coarsening time t. Straight line displays best fit through the data.

size distribution was found to be unchanged with coarsening time and temperature. The $\bar{r}^3(t)$ data were best fitted with the coarsening rate $K = (55 \pm 4)$ nm^3 s^{-1} for 773 K. From the two data points at 723 K the coarsening rate $K = 21$ nm^3 s^{-1} was approximated. Extrapolation of the linear dependence to $t = 0$ leads one to expect that r_0 is relatively small, which would indicate slow growth of the drops in the previous nucleation stage.

B. Viscosity

The temperature dependence of viscosity of the demixed glass PB2 and the homogeneous glass PB3 is shown in Fig. 5. Within the narrow temperature range the viscosity data (η in Pa s) were fitted by the Arrhenian parameters $A = -30.5$, $B = 30\,474$ K (PB2) and $A = -32.6$, $B = 31\,499$ K (PB3) according to $\log \eta = A + B/T$. Inspection of Fig. 5 reveals a slightly lower effective viscosity of the demixed glass PB2 as compared to the homogeneous glass PB3, which indicates rheometric regimes of capillary numbers close to unity during compression of the glass cylinders. The viscosity ratio κ of Eq. (6) was derived from Fig. 5 by taking the viscosity of the homogeneous glass PB3 (B_2O_3 content of PB3 was close to the binodal composition) as the viscosity of the matrix, while the viscosity of pure boron trioxide glass[48] was used as the drop viscosity of demixed PB1 and PB2 glasses.

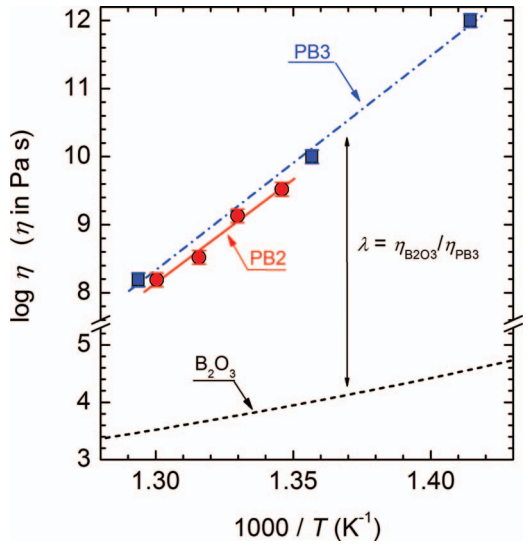

FIG. 5. Viscosity as a function of temperature of demixed glass PB2 and homogeneous glass PB3. Viscosity temperature curve of pure boron trioxide glass from Dietzel and Brückner.[48]

C. Liquid-liquid interfacial energy

To find the diffusion coefficient of the coarsening process, the liquid-liquid interfacial energy σ_{ll} was determined firstly. Therefore we used Eq. (6), the viscosity ratio κ, the drop ovality δ, and the corresponding effective strain rate $\dot{\varepsilon}_{yz}$ of Table I. The results show that σ_{ll} was constant within the uncertainty of the measurements. Therefore, an average value of (0.017 ± 5) J m^{-2} was used for the calculation of D_K, for which we assume that the entropy contributions to σ_{ll} were negligible due to the quasi constant binodal compositions in the temperature range under consideration.

D. Diffusivity

Assuming diffusion controlled coarsening in the demixed glass PB1 the diffusion coefficient $D_K = (9 \pm 5) \times 10^{-17}$ m^2 s^{-1} was determined using Eq. (10), the coarsening rate $K = 55 \pm 4$ nm^3 s^{-1}, $\phi(0.12) = 1.8$,[36,37] the binodal compositions $c^{\alpha}{}_{B_2O_3} = 80.1\%$, $c^{\beta}{}_{B_2O_3} = 99.9\%$ (Fig. 1), and the molar volume $V_M = 37.616$ cm^3 mol^{-1} at 773 K. V_M was calculated from the room temperature density[16] and molar weight of the drop glass. Herein the contribution of thermal expansion to the molar volume was negligible. The diffusivity was also determined for coarsening of the drop population at 723 K. Using again Eq. (10) and the data: $K = 21$ nm^3 s^{-1}, $\phi(0.12) = 1.8$,[36,37] $c^{\alpha}{}_{B_2O_3} = 80.04\%$, $c^{\beta}{}_{B_2O_3} = 99.96\%$ (Fig. 1), and $V_M = 37.625$ cm^3 we calculated $D_K = (3 \pm 1) \times 10^{-17}$ m^2 s^{-1}.

V. DISCUSSION

Emulsion rheology was applied to determine the interfacial energy in demixed lead borate melts independently from coarsening theory. For the small temperature range and the experimental scatter this parameter was treated as a constant. However, we note that σ_{ll} shows in general a negative temperature dependence, i.e., follows the relation $\sigma = \sigma_0 (1 - (T/T_c))^{\gamma}$ where σ_0 and γ are constants and T_c is the critical temperature of the demixed glass system under consideration.[53] The decrease in interfacial energy with increasing T/T_c results commonly from the decrease in the difference of the binodal compositions. In contrast, the lead borate immiscibility dome (Fig. 1) exhibits almost vertical branches in the considered temperature range for which compositional effects of σ_{ll} were negligible. The value of 0.017 J m^{-2} was by the factor of

TABLE II. Diffusivity in PbO-B_2O_3 glasses at 773 and 723 K. Data: Coarsening (Eq. (10)) in demixed PB1 glass ($c^0_{B_2O_3}$ = 82.2 mol. %); ^{18}O self-diffusivity in boron trioxide glass ($c^0_{B_2O_3}$ = 100 mol. %);[58] ^{18}O self-diffusivity PbO-rich lead borate glass (c^0_{B2O3} = 31 mol. %);[57] ^{207}Pb self-diffusivity in lead diborate glass ($c^0_{B_2O_3}$ = 66.7 mol. %).[56] Eyring diffusivity of matrix glass in demixed PB1 and PB2 glasses was calculated using Eqs. (7) and (8) with CN = 1 and $(V_M/(mN_A))^{1/3}$ = 240 pm. Number in parenthesis gives uncertainty of the last digit.

	Diffusivity $D \times 10^{17}$ (m^2 s^{-1})				
T (K)	Coarsening Eq. (10)	^{207}Pb self-diffusion[a]	^{18}O self-diffusion[b]	^{18}O self-diffusion[c]	Eyring η_m Eq. (7)
773	9(5)	14.1[d]	4.8[e]	33.1	0.032
723	3(1)	7.6	2.9[e]	144.1	0.000047

[a]Reference 56.
[b]Reference 57.
[c]Reference 58.
[d]Extrapolated from 752 K.
[e]Extrapolated from 698 K.

7 smaller as previously estimated for this system,[9] but 3.7 times larger than determined from the critical drop sizes in the soda-lime silica system.[8]

Knowing σ_{ll} of the demixed PB1 glass the diffusivity of the final competitive drop growth was calculated without assuming interfacial properties. In order to shed light on the diffusion mechanism, i.e., the nature of the diffusing species controlling the coarsening rate, we derived Eyring diffusivities from the viscosity data and analyzed self-diffusion data of the constituting lead and oxygen ions from literature. The former led to the diffusion coefficients $D_{\eta\text{-}matrix}$ = 3.2 × 10^{-19} m^2 s^{-1} and 4.7 × 10^{-22} m^2 s^{-1} (using Eqs. (7) and (8), Cn = 1 and $(V_M/(mN_A))^{1/3}$ = 240 pm) for a viscosity coupled coarsening process through the PbO-rich matrix at 773 and 723 K, respectively. Within the B_2O_3 rich drop glass Eyring diffusivity results $D_{\eta\text{-}drop}$ = 1.5 × 10^{-14} m^2 s^{-1} (773 K) and $D_{\eta\text{-}drop}$ = 2.3 × 10^{-15} m^2 s^{-1} (723 K), which is of course much faster than the mobility in the matrix glass. Hereby we took the viscosity of the drop melt (nearly pure B_2O_3) into considerations as an approximate value for the dynamics of the boron-oxygen bonds in the matrix glass, since to our knowledge, boron diffusivities in lead borate melts have not been reported. The error of this oversimplified approach to boron mobility is mainly due to the different structural roles of boron in pure B_2O_3 and different borate glasses, i.e., boron is unique in readily transforming between three (^{III}B) and four (^{IV}B) coordination with changes in composition,[24] temperature,[54] and pressure.[55] Tracer diffusivity data in lead borate melts resulted in $D_{207\text{-}Pb}$ = 1.4 × 10^{-16} (773 K) and $D_{207\text{-}Pb}$ = 7.6 × 10^{-17} (723 K) for lead[56] and $D_{18\text{-}O}$ = 4.8 × 10^{-17} m^2 s^{-1} (773 K) and $D_{18\text{-}O}$ = 2.9 × 10^{-17} m^2 s^{-1} (723 K) for oxygen diffusion.[57] Herein the ^{207}Pb diffusivities in the range from 548 K to 698 K[56] and of ^{18}O diffusivities in the range from 673 K to 753 K[57] were extrapolated using Eq. (9) to 723 and 773 K, respectively. The diffusivities were compiled together with ^{18}O diffusivities in pure boron trioxide glasses[58] in Table II. In order to bring the viscosity-derived diffusivity with the coarsening diffusivity in agreement, the assumed jump distance has to be divided by the factor $f_{\eta\text{-}matrix}$ = $\lambda_{\eta\text{-}matrix}/\lambda_K = D_K/D_{\eta\text{-}matrix} \approx$ 281 (773 K), 63 830 (723 K). This would of course result in physically unrealistic small values of Cn ($Cn_{\eta\text{-}matrix} < 0.004$, Fig. 6) and sizes of the activated complex, respectively.

Decoupling of the coarsening kinetics from the characteristic time scales of cooperative rearrangements of the glass network would not only imply much faster time scales than those of the dynamic of bond breakage of bridging oxygen but also a smaller energy barrier related with the coarsening mechanism. Therefore, we scaled ion and coarsening diffusivity with viscosity for each melt in a double logarithmic diagram (Fig. 6). Viscosity data were taken from Dietzel and Brückner[16] for the pure B_2O_3 and from Nemilov and Romanova[59] for the binary lead borate melts. The coarsening diffusivity was scaled with the viscosity of PB3 glass, which resembles the matrix composition of the demixed PB1 and PB2 glasses. From inspection of Fig. 6 we extracted the following trend: At high viscosities ($\eta > 10^7$ Pa s) oxygen and lead were diffusing much faster than the corresponding

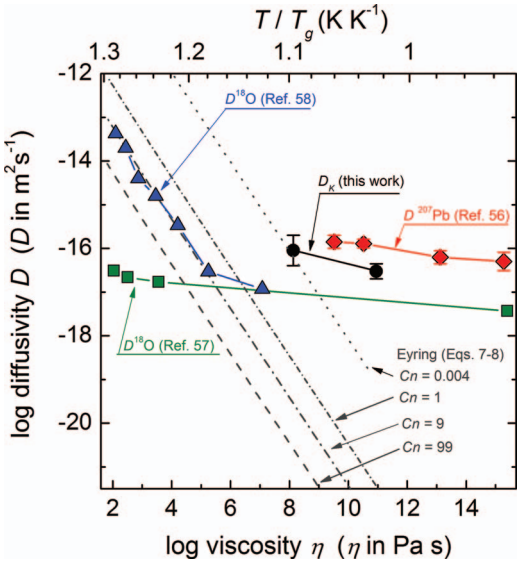

FIG. 6. Diffusivity vs. viscosity in the PbO-B_2O_3 glass system using double logarithmic scales. Data: D_K = Diffusivity of the coarsening process (Eq. (10)) and viscosity of matrix glass (Fig. 5) in demixed PB1 glass ($c^0_{B_2O_3}$ = 82.2 mol. %); ^{18}O self-diffusivity[58] and viscosity[16] in boron trioxide glass ($c^0_{B_2O_3} \approx$ 100 mol. %); ^{18}O self-diffusivity[57] and viscosity[59] in PbO-rich lead borate glass ($c^0_{B_2O_3}$ = 31 mol. %); ^{207}Pb self-diffusivity[56] and viscosity[59] in lead diborate glass ($c^0_{B_2O_3}$ = 66.7 mol. %). Eyring diffusivity calculated using Eqs. (7) and (8) for $(1 + Cn)$ = 1.004, 2, 10, and 100 species per activated complex and $(V_M/(mN_A))^{1/3}$ = 240 pm. Upper x-coordinate scales diffusivity with the relative temperature T/T_g of the matrix glass of the demixed PB1 and PB2 glasses (T_g = 706 K).

network dynamics, while for smaller viscosities ($\eta < 10^7$ Pa s) oxygen seems to follow the network mobility. However, differences in the actual glass composition of the viscosity and diffusivity data-sets compiled from different investigators may contribute to the shift of the ^{18}O-data in case of the lead-rich borate glass with $c^0_{B_2O_3} = 31$ mol. %. Coarsening seems to follow the ionic trend resulting in up to 4 orders of magnitude larger diffusion rates than those derived from viscosity of the matrix glass.

On the other hand scaling the matrix viscosity with the reduced temperature T/T_g (top x-coordinate of Fig. 6) shows that the onset of decoupling falls in the temperature range from 1.1 to 1.2 T_g. A similar onset temperature for the breakdown of the Eyring relation was reported for the crystal growth kinetics in silicate glasses.[60,61] The origin of decoupling was assigned to spatially dynamic heterogeneity in the deeply supercooled silicate liquid.[62] We note that a decrease or an increase in σ_{ll} by a factor of 10 would change log D_K only by ± 1. Thus, the discrepancy between the upper and lower value of σ_{ll}[8,9] cannot explain the deviation (breakdown) at $T < 1.1\ T_g$ of Fig. 6.

Further, we performed an Arrhenius analysis of the temperature dependence of the coarsening rate constant K (not shown). An approximate value of the coarsening enthalpy of ≈ 90 kJ mol^{-1} was obtained from the slope of an straight line and assuming linear dependence of ln K with $1/T$ (coarsening rate constants were only determined from drop distributions at 723 K and 773 K). Utilizing the Arrhenian viscosity parameter B (see Sec. III B) we approximated the degree of decoupling by the ratio $E_K/E_\eta \approx 0.15$, where E_K and E_η are the activation energies for coarsening and viscous flow, respectively. In silicate glasses decoupling ratios close to this value (0.13–0.16) were reported for the mobility of network modifying cations to the dynamics of the network at the glass transition temperature.[51,63] Taking into account the structural role of Pb^{2+} as a charge compensator for tetrahedrally coordinated boron, it is most likely that coarsening is controlled by dynamics of the interaction between Pb^{2+} cations and $(BO_4)^-$ units of polyborate groups.

VI. CONCLUSIONS

Boron oxide-rich drops in a lead oxide-rich matrix were developed by liquid-liquid phase separation in a lead borate glass due to annealing above the two glass transitions temperatures. We found that the final drop-in-matrix structure resulted from competitive growth, i.e., the mean size of the drop population followed the cube root time dependence characteristic for diffusion controlled coarsening. The diffusivity of the coarsening process was determined using coarsening rate and liquid-liquid interfacial energy data and compared with those of tracer diffusion experiments and Eyring diffusivities of viscous flow. We found that the coarsening kinetics in the demixed lead-borate melt was up to 4 orders of magnitude faster than the time scales of network mobility, i.e., a decoupling of the coarsening dynamics from that of viscous flow was evident. The low activation energy and the fast dynamic of the coarsening process indicate a short-range transport mechanism in the glass structure rather than cooperative rearrangements of intermediate range at temperatures in the glass transition range ($T < 1.1\ T_g$).

ACKNOWLEDGMENTS

The financial support of the Deutsche Forschungsgemeinschaft (DFG) under Grant No. De598/10-1 is gratefully acknowledged.

[1] J. Zarzycki and F. Naudin, Phys. Chem. Glasses **8**, 11 (1967).
[2] U. Lembke and W. Blau, Ber. Bunsenges. Phys. Chem. **100**, 1651 (1996).
[3] D. G. Burnett and R. W. Douglas, Phys. Chem. Glasses **11**, 125 (1970).
[4] F. Gauthier and J. Gombert, J. Non-Cryst. Solids **49**, 157 (1982).
[5] K. Yata and T. Yamaguchi, J. Am. Ceram. Soc. **75**, 2010 (1992).
[6] B. R. Wheaton and A. G. Clare, J. Non-Cryst. Solids **353**, 4767 (2007).
[7] J. Deubener, Z. A. Osborne, and M. C. Weinberg, J. Non-Cryst. Solids **215**, 252 (1997).
[8] J. J. Hammel, J. Chem. Phys. **46**, 2234 (1967).
[9] L. Wondraczek, J. Deubener, H. del Pozo, and A. Habeck, J. Am Ceram. Soc. **88**, 1673 (2005).
[10] R. F. Geller and E. N. Bunting, J. Res. Natl. Bur. Stand. **18**, 585 (1937).
[11] C. Kröger and K. Lieck, Z. Anorg. Allg. Chem. **279**, 300 (1955).
[12] D. J. Liedberg, C. G. Ruderer, and C. G. Bergeron, J. Am. Ceram. Soc. **48**, 440 (1965).
[13] J. Podlesny, M. C. Weinberg, G. F. Neilson, and A. Chen, J. Mater. Sci. **28**, 1663 (1993).
[14] P. B. Macedo and J. H. Simmons, J. Res. Natl. Bur. Stand. **78A**, 53 (1974).
[15] J. H. Simmons, J. Am. Ceram. Soc. **56**, 284 (1973).
[16] R. R. Shaw and D. R. Uhlmann, J. Non-Cryst. Solids **1**, 474 (1969).
[17] A. Habeck, H. Hessenkemper, and R. Brückner, Glastech. Ber. **63**, 111 (1990).
[18] H. Reiß, Glastech. Ber. **70**, 224 (1997).
[19] H. Reiß, Glastech. Ber. **71**, 300 (1998).
[20] D. Zhu, C. S. Ray, F. Luo, W. Zhou, and D. E. Day, Ceram. Int. **34**, 417 (2008).
[21] J. E. Shelby, J. Non-Cryst. Solids **49**, 287 (1982).
[22] S. Inoue, K. Wada, A. Nukui, M. Yamane, S. Shibata, A. Yasumori, T. Yano, A. Makishima, H. Inoue, M. Uo, and Y. Fujimori, J. Mater. Res. **10**, 1561 (1995).
[23] K. S. Kim and P. J. Bray, J. Chem. Phys. **64**, 4459 (1976).
[24] J. L. Shaw, U. Werner-Zwanziger, and J. W. Zwanziger, Phys. Chem. Glasses: Eur. J. Glass Sci. Technol. B **47**, 513–517 (2006).
[25] C. Gautam, A. K. Yadav, and A. K. Singh, ISRN Ceramics **2012**, 428497.
[26] I. M. Lifshitz and V. V. Slyozov, J. Phys. Chem. Solids **19**, 35 (1961).
[27] C. Wagner, Z. Elektrochem. **65**, 581 (1961).
[28] L. Ratke and W. K. Thieringer, Acta Metal. **33**, 1793 (1985).
[29] A. J. Ardell, Acta Metal. **20**, 61 (1972).
[30] A. D. Brailsford and P. Wynblatt, Acta Metal. **27**, 489 (1979).
[31] C. K. L. Davies, P. Nash, and R. N. Stevens, Acta Metal. **28**, 179 (1980).
[32] K. Tsumaraya and Y. Mityata, Acta Metal. **31**, 437 (1983).
[33] J. A. Marqusee and J. Ross, J. Chem. Phys. **80**, 536 (1984).
[34] M. Tokuyama and K. Kawasaki, Physica A **123**, 386 (1984).
[35] P. W. Voorhees and M. E. Glicksman, Acta Metal. **32**, 2001 (1984).
[36] P. W. Voorhees and M. E. Glicksman, Acta Metal. **32**, 2013 (1984).
[37] P. W. Voorhees, J. Stat. Phys. **38**, 231 (1985).
[38] A. Baldan, J. Mater. Sci. **37**, 2171 (2002).
[39] H. Eyring, D. Henderson, B. J. Stover, and E. M. Eyring, *Statistical Mechanics and Dynamics*, 2nd ed. (Wiley, New York, 1982), p. 785.
[40] R. J. Eagan and C. G. Bergeron, J. Am. Ceram. Soc. **55**, 53 (1972).
[41] T. Takamori and M. Tomozawa, J. Am. Ceram. Soc. **59**, 377 (1976).
[42] J. Deubener, F. de Moraes, and R. Brückner, J. Non-Cryst. Solids **219**, 57 (1997).
[43] J. Deubener and L. Wondraczek, in *Proceedings of the 106th Annual Meeting of the American Ceramic Society, Indianapolis, IN, 18–21 April 2004* [Ceram. Trans. **170**, 47 (2004)].
[44] F. K. Chen and C. J. Chen, Trans. ASME **122**, 192 (2000).
[45] A. N. Gent, Br. J. Appl. Phys. **11**, 85 (1960).
[46] R. W. Douglas, W. L. Amstrong, J. P. Edward, and D. Hall, Glass Technol. **6**, 52 (1965).
[47] R. Brückner and G. Demharter, Glastechn. Ber. **48**, 12 (1975).

[48]A. Dietzel and R. Brückner, Glastech. Ber. **28**, 455 (1955).
[49]N. Böse, G. Klingenberg, and G. Meerlender, Glastech. Ber. **74**, 115 (2001).
[50]S. Zietka, J. Deubener, H. Behrens, and R. Müller, Phys. Chem. Glasses: Eur. J. Glass Sci. Technol. B **48**, 380 (2007).
[51]J. Deubener, H. Bornhöft, S. Reinsch, R. Müller, J. Lumeau, L. N. Glebova, and L. B. Glebov, J. Non-Cryst. Solids **355**, 126 (2009).
[52]E. E. Underwood, *Quantitative Stereology* (Addison-Wesley Publication, Reading, 1970), p. 109.
[53]J. W. P. Schmelzer, J. Schmelzer, and I. S. Gutzow, J. Chem. Phys. **112**, 3820 (2000).
[54]L. Wondraczek, S. Sen, H. Behrens, and R. E. Youngman, Phys. Rev. B **76**, 014202 (2007).
[55]J. Wu, J. Deubener, J. F. Stebbins, L. Grygarova, H. Behrens, L. Wondraczek, and Y. Yue, J. Chem. Phys. **131**, 104504 (2009).
[56]J. P. DeLuca and C. G. Bergeron, J. Am. Ceram. Soc. **52**, 629 (1969).
[57]H. A. Schaeffer and H. J. Oel, Glastech. Ber. **42**, 493 (1969).
[58]T. Tokuda, T. Ito, and T. Yamagushi, Z. Naturforsch. **26**, 2058 (1971).
[59]S. V. Nemilov and N. V. Romanova, Neorg. Mater. **5**, 1247 (1969).
[60]M. L. F. Nascimento, E. B. Ferreira, and E. D. Zanotto, J. Chem. Phys. **121**, 8924 (2004).
[61]M. L. F. Nascimento and E. D. Zanotto, J. Chem. Phys. **133**, 174701 (2010).
[62]M. L. F. Nascimento, V. M. Fokin, E. D. Zanotto, and A. S. Abyzov, J. Chem. Phys. **135**, 194703 (2011).
[63]J. Deubener, Y. Z. Yue, H. Bornhöft, and M. Ya, Chem. Geol. **256**, 299 (2008).